ChemPhysChem

Chemistry Europe
European Chemical Societies Publishing

Accepted Article

Title: Chirality without Stereoisomers: Insight from the Helical Response of Bond Electrons

Authors: Samantha Jenkins, Tianlv Xu, Xing Nie, Shuman Li, Yong Yang, Herbert Früchtl, Tanja van Mourik, Steven R. Kirk, Martin J. Paterson, and Yasuteru Shigeta

To be cited as: *ChemPhysChem* 10.1002/cphc.202100397

Link to VoR: https://doi.org/10.1002/cphc.202100397

WILEY-VCH

10.1002/cphc.202100397

Chirality without Stereoisomers: Insight from the Helical Response of Bond Electrons

Tianlv Xu[1], Xing Nie[1], Shuman Li[1], Yong Yang[1], Herbert Früchtl[2], Tanja van Mourik[2], Steven R. Kirk[*1], Martin J. Paterson[3], Yasuteru Shigeta[4] and Samantha Jenkins[*1]

[1]*Key Laboratory of Chemical Biology and Traditional Chinese Medicine Research and Key Laboratory of Resource National and Local Joint Engineering Laboratory for New Petro-chemical Materials and Fine Utilization of Resources, College of Chemistry and Chemical Engineering, Hunan Normal University, Changsha, Hunan 410081, China*

[2]*EaStCHEM School of Chemistry, University of Saint Andrews, North Haugh, St Andrews, Fife KY16 9ST, Scotland, United Kingdom.*

[3]*Institute of Chemical Sciences, School of Engineering and Physical Sciences, Heriot-Watt University, Edinburgh, EH14 4AS, UK*

[4]*Center for Computational Sciences, University of Tsukuba, Tsukuba 305-8577, Japan*

email: steven.kirk@cantab.net
email: samanthajsuman@gmail.com

The association between molecular chirality and helical characteristics known as the chirality-helicity equivalence is determined, for the first time, by quantifying a chirality-helicity measure consistent with photoexcitation circular dichroism experiments. This is demonstrated using a formally achiral S_N2 reaction and a chiral S_N2 reaction. Both the achiral and chiral S_N2 reactions possess significant values of the chirality-helicity measure and display a Walden inversion, i.e. an inversion of the chirality between the reactant and product. We also track the chirality-helicity measure along the reaction path and discover the presence of chirality at the transition state and two intermediate structures for both reactions. We demonstrate the need for the chirality-helicity measure to differentiate between steric effects due to eclipsed conformations and chiral behaviors in formally achiral species. We explain the significance of this work for asymmetric synthetic reactions including the intermediate structures where the Cahn–Ingold–Prelog (CIP) rules cannot be used.

1. Introduction

A chiral molecule usually has at least one chiral center and the Cahn–Ingold–Prelog (CIP) priority rules determine the chiral configuration (R/S) without calculations[1,2] : these rules have recently been updated[3]. There are however, optical isomers of coordination compounds used as stereoselectivity catalysts for which the chirality cannot be assigned from the CIP rules. The existence of chirality has important implications[4–6] and the origin of chiral asymmetry[7] in molecular biology is one of the great mysteries in the understanding of the origin of life[8–15]. Recent investigations of structural chirality include those of DNA-stabilized silver clusters with circular dichroism spectra[16] and investigations of interlocked molecules, widely observed in biomacromolecules[17]. In 1848 Louis Pasteur proposed biomolecular homochirality as a possible simple 'chemical signature of life[18]. More recently, the subject was considered by Prelog[4] and by Quack[19,20]. Quack concluded from extensive theoretical investigations that no direct relationship between energy difference and the handedness of a chiral molecule exists, as would be expected, for an L-amino acid dominant world.

Helical characteristics of stereoisomers were first proposed as the origin of chirality by Fresnel[21] in 1851. This was later demonstrated by optical experiments that show materials having different refractive indices for right (R) and left (S) circularly polarized light, which is known as circular dichroism[22], consistent with theories of optical activity that correlate the inherent helical identities with direction of rotation of the circularly polarized light[23–25]. Much later, a 'helix theory' for molecular chirality and chiral interaction was hypothesized by Wang, who understood that evidence for this helical character was not provided by molecular geometries[26], nor was this character solely attributable to steric hindrance. The association between helical characteristics and chirality was referred to as the 'chirality-helicity equivalence' by Wang. The need for a better understanding of the behavior of the charge density redistribution was demonstrated in recent experiments by Beaulieu *et al.* on neutral molecules[27] that utilize coherent helical motion of bound electrons, consistent with our previous work[28]. Recently, Banerjee-Ghosh *et al.* also demonstrated that the charge density redistribution in chiral molecules, not spatial effects[29], is responsible for an enantiospecific preference in electron spin orientation, consistent with Wang[26]. Earlier[30], the interdependence of steric-electronic factors was reported to be more complex than that discernable from molecular structures alone, as was also the case for the helical electronic transitions of spiroconjugated molecules[31].

The unknown chirality-helicity equivalence was recently located, but not quantified, for chiral compounds by some of the current authors[28], who were able to differentiate the S and R stereoisomers consistent with the naming schemes from optical experiments. The insufficiency of conventional (scalar) QTAIM[32] (quantum theory of atoms in molecules) for distinguishing S and R stereoisomers was also demonstrated. If on applying a bond torsion, a helical response of the electronic charge density distribution is present, then both non-axial (perpendicular to the bond-path) and axial (parallel to the bond-path) displacements of the torsional C1-C2 bond critical point will be found.

The human olfactory, gustatory and metabolic systems are selective towards molecular stereoisomers. Consequently, asymmetric synthesis, the selective synthesis of either the left or right-handed stereoisomers, is important from the viewpoint of pharmaceutical development, in addition to other chemical industries. The prediction of asymmetric synthetic reactions is one of the most fundamental problems in industrial organic and catalytic chemistry[33,34] and S_N2 reactions are basic building blocks of organic synthesis. These have stereochemistry as a fundamental feature through the possibility to invert or retain the configuration at the chiral center, depending on frontside or rearside nucleophilic attack. S_N2 reactions in general are highly stereospecific and quantifying fundamental aspects relating to these is an important step towards asymmetric synthesis.

In this investigation we use Bader's formulation of the stress tensor[35] and NG-QTAIM (next generation QTAIM) on the basis of the superior performance of the stress tensor compared with vector-based QTAIM in terms of more effectively distinguishing the S and R stereoisomers of lactic acid[36]. We will provide, for the first time, a measure to quantify the chirality-helicity equivalence by calculating the helicity (the axial displacement), that has previously not been identified, and combining with the chirality (the non-axial displacement) to form a chirality-helicity measure. We will apply this chirality-helicity measure to a chiral S_N2 reaction and a formally achiral S_N2 reaction to investigate the effect of a front-side nucleophilic attack. We will also determine the chirality-helicity measure in a range of achiral molecules to differentiate the presence of steric and chiral behaviors.

2. Theoretical Background and Computational Details

The background of QTAIM and next generation QTAIM (NG-QTAIM)[37–43] with explanations is provided in the **Supplementary Materials S1**, along with the procedure to generate the stress tensor trajectories $\mathbb{T}_\sigma(s)$. In this investigation we will use Bader's formulation of the stress tensor[35] within the QTAIM partitioning, which is a standard option in the QTAIM AIMAll[44] suite. The ellipticity, ε, quantifies the relative accumulation of the electronic charge density $\rho(\mathbf{r_b})$ in the two directions perpendicular to the bond-path at a Bond Critical Point (*BCP*) with position $\mathbf{r_b}$. The ellipticity ε is defined as $\varepsilon = |\lambda_1|/|\lambda_2| - 1$ and for values of the ellipticity $\varepsilon > 0$, the λ_1 and λ_2 eigenvalues of the Hessian of $\rho(\mathbf{r})$ are associated with the shortest and longest axes of the elliptical distribution of $\rho(\mathbf{r_b})$ respectively. The most (facile) preferred direction of electron charge density accumulation determines the direction of bond displacement[45]. Later, Bone and Bader proposed that when a structure is slightly perturbed, the direction of displacement of the electrons coincides with that of the atoms[46]; this was subsequently confirmed[47,48].

The calculation of the stress tensor trajectory, $\mathbb{T}_\sigma(s)$, where s indicates a reaction coordinate that is mapped onto a $\mathbb{U}_\sigma$-space, was previously[28] used to established the $\mathbb{T}_\sigma(s)$ classifications of S and R stereoisomers for lactic acid and alanine, consistent with optical experiment classification schemes. The $\mathbb{T}_\sigma(s)$ comprise a series of contiguous points and is a 3-D vector path that displays the effect of the structural change, i.e. the

bond torsion $0.0^o \leq \theta \leq 180.0^o$ counterclockwise (CCW) or $-180.0^o \leq \theta \leq 0^o$ clockwise (CW). Note, the $\mathbb{T}_\sigma(s)$ are constructed at the torsional *BCP* for a torsion $\theta = 0.0^o$ which corresponds to the *minimum energy* geometry. The CCW and CW directions of torsion indicate left- and right-handed directions of bond torsion respectively, consistent with optical experiment S and R stereoisomer classification schemes. The $\mathbb{T}_\sigma(s)$ are constructed using the changes in position **dr** of the *BCP* for all torsional displacement steps of the calculation. The chirality-helicity measure $\mathbb{C}_{helicity}$ of the $\mathbb{T}_\sigma(s)$ is formed from the simple arithmetic product of the chirality $\mathbb{C}_\sigma$ and the helicity $\mathbb{B}_\sigma$. The chirality $\mathbb{C}_\sigma$ is formed from the $\underline{\mathbf{e}}_{1\sigma}\cdot\mathbf{dr}$ (→ bond-twist) *BCP* shift in the plane perpendicular to $\underline{\mathbf{e}}_{3\sigma}$ (the bond-path). The helicity $\mathbb{B}_\sigma$ is formed from the axial *BCP* sliding $\mathbf{e}_{3\sigma}\cdot\mathbf{dr}$ (→ bond-anharmonicity)[49], where the *BCP* sliding is the shift of the *BCP* position along the containing bond-path due to changes to bonded inter-nuclear separations. The presence of a helical response, i.e. non-zero value of $\mathbb{C}_{helicity}$, of the torsional *BCP* to the applied torsion θ, is determined by $\mathbb{B}_\sigma \neq 0$ and may not necessarily coincide with a helical $\mathbb{T}_\sigma(s)$, except for the limited case of some conventionally chiral molecules such as lactic acid and alanine.

Computational Details

For the achiral S_N2 reaction, we modelled the nucleophilic attack of Br^- on monochloroethane resulting in monobromoethane, with Cl^- ejected as the leaving group and its chiral equivalent, with one hydrogen attached to reference carbon atom C1 (indicated by the blue encircled C1 atoms in **Figures 1-2**)) of monochloroethane replaced by a phenyl group to give the corresponding chiral S_N2 reaction. All computations were performed using Gaussian 09E01[50]. We used the B3LYP DFT functional with the 6-311++G(2d,3p) basis set, a combination previously tested to give accurate total electronic charge density distributions suitable for QTAIM analysis, with negligible BSSE effects[28]. Computation of the two-electron integrals used a 'superfine' (pruned 175,974/250,974) grid with a two-electron integral accuracy of 10^{-14} and an SCF convergence criterion of 10^{-10}. All subsequent wavefunction, geometry-optimization, torsion and IRC (intrinsic reaction coordinate) calculations were carried out with these settings. As one of the reactants and one of the products is negatively charged, the system was treated as having a total charge of -1. We geometry-optimized using Cartesian coordinates (tight convergence criteria) from archived data[51] and verified the transition state. The full IRC computation used a maximum step size of 0.1 Bohr and recalculation of the full force-constant matrix every five steps. Initial and final uncharged (charge 0) structures in absence of the unbound halogen ion were geometry-optimized, starting from each converged IRC endpoint geometry respectively.

The first step of the computational torsional protocol is to perform a constrained scan of the potential energy surface (ΔE). The scan was performed with a constrained (Z-matrix) geometry optimization performed at all steps with all coordinates free to vary except for the torsion coordinate θ. We determine the direction of torsion as $0.0^o \leq \theta \leq 180.0^o$ (CCW) or $-180.0^o \leq \theta \leq 0^o$ (CW) from an increase or a decrease in the dihedral

angle respectively. Single-point calculations were then performed on each scan geometry using the same computational method, converged to $< 10^{-10}$ RMS change in the density matrix and $< 10^{-8}$ maximum change in the density matrix to yield the final wavefunctions for analysis. QTAIM and stress tensor analysis was performed with the AIMAll[44] suite on each wavefunction obtained in the previous step. All molecular graphs were additionally confirmed to be free of non-nuclear attractor critical points.

We also considered two intermediate structures on each of the achiral and chiral IRCs, dubbed INTS1 and INTS2, which correspond to the peaks of the RMS energy gradient norm on either side of the transition state. For the chiral reaction, all dihedral torsion angle definitions started on the first phenyl carbon and consistently ended on the same hydrogen (C9-C1-C2-H4 for TS, INTS1, INTS2 and C8-C1-C2-H5 for the isolated product and reactant). For the transition state (TS) and intermediate structures (INTS1 and INTS2), during the torsions both C1-halogen bond distances were additionally fixed to their IRC path structure values. For the achiral reaction, the equivalent (to the chiral reaction) dihedrals were (H3-C1-C2-H6) for the TS, INTS1 and INTS2 and (H3-C1-C2-H7 and H3-C1-C2-H6) for the isolated endpoint structures.

3. Results and discussions

The chirality-helicity measure $\mathbb{C}_{helicity}$ for formally achiral and chiral species

We now consider the formally achiral S_N2 reaction of the nucleophilic attack of Br^- on monochloroethane (reactant) resulting in monobromoethane (product), with Cl^- ejected as the leaving group, see **Figure 1** and its chiral equivalent, with one hydrogen attached to carbon C1 of monochloroethane replaced by a phenyl group, see **Figure 2**. The relative energy ΔE plots, ellipticity ε profiles and stress tensor trajectories $\mathbb{T}_\sigma(s)$ for the torsions θ, $-180.0^o \leq \theta \leq +180.0^o$, where the C1-C2 *BCP* is the torsion *BCP* used for the entries of **Tables 1-2** are provided in the **Supplementary Materials S2-S3**. The chirality $\mathbb{C}_\sigma$ quantifies the *non-axial* displacement of the *BCP* and is defined as the difference (CCW minus CW) of the bond-twist$_{max}$ component of the $\mathbb{T}_\sigma(s)_{max}$, see **Tables 1-2**. The sign (+ or -) of the chirality $\mathbb{C}_\sigma$ determines the presence of $\mathbf{S_\sigma}$ ($\mathbb{C}_\sigma > 0$) and $\mathbf{R_\sigma}$ ($\mathbb{C}_\sigma < 0$) character; note the use of the subscript "$_\sigma$" for $\mathbf{S_\sigma}$ and $\mathbf{R_\sigma}$ because the $\mathbb{C}_\sigma$ and $\mathbb{B}_\sigma$ are calculated using the stress tensor $\mathbb{T}_\sigma(s)$, see **Tables 1(b)-2(b)**. The chiral asymmetry (helicity) $\mathbb{B}_\sigma$ quantifies the degree of *axial* displacement *BCP* along the bond-path and defined as the difference (CCW minus CW) of the bond-anharmonicity$_{max}$ component of the $\mathbb{T}_\sigma(s)_{max}$. The helicity $\mathbb{B}_\sigma$ is the response to the bond torsion, i.e. the sliding of the *BCP* along the bond-path[49]. Values of the helicity $\mathbb{B}_\sigma > 0$ indicate dominant $\mathbf{S_\sigma}$ character, whereas the converse is true for $\mathbb{B}_\sigma < 0$. The chirality-helicity measure $\mathbb{C}_{helicity} = \mathbb{C}_\sigma\mathbb{B}_\sigma$ is defined as the simple arithmetic product of the non-axial ($\mathbb{C}_\sigma$) and axial ($\mathbb{B}_\sigma$) contributions of the *BCP* displacement in response to the torsion θ.

We track the change in the chirality-helicity measure $\mathbb{C}_{helicity}$ throughout the progress of the IRC pathway that includes the reactant, product and transition state (TS), see **Figure 1(a).** We also include two

intermediate structures on each of the achiral and chiral IRCs, namely INTS1 and INTS2, that correspond to the peaks of the RMS energy gradient norm on either side of the transition state, to capture the atomic rearrangement process of the Walden inversion, see **Figure 1(b)** and **Figure 2(b)** respectively. The magnitude of the $\mathbb{C}_{helicity}$ for the reactants and products of the achiral and chiral reactions are similar, compare **Table 1(b)** with **Table 2(b)**. The value of the $\mathbb{C}_{helicity}$ for the transition state of the achiral reaction is significantly lower than for the chiral reaction as may be expected, although the $\mathbb{C}_{helicity}$ value for INTS2 of the achiral reaction is significantly higher than for the INTS2 of the chiral reaction.

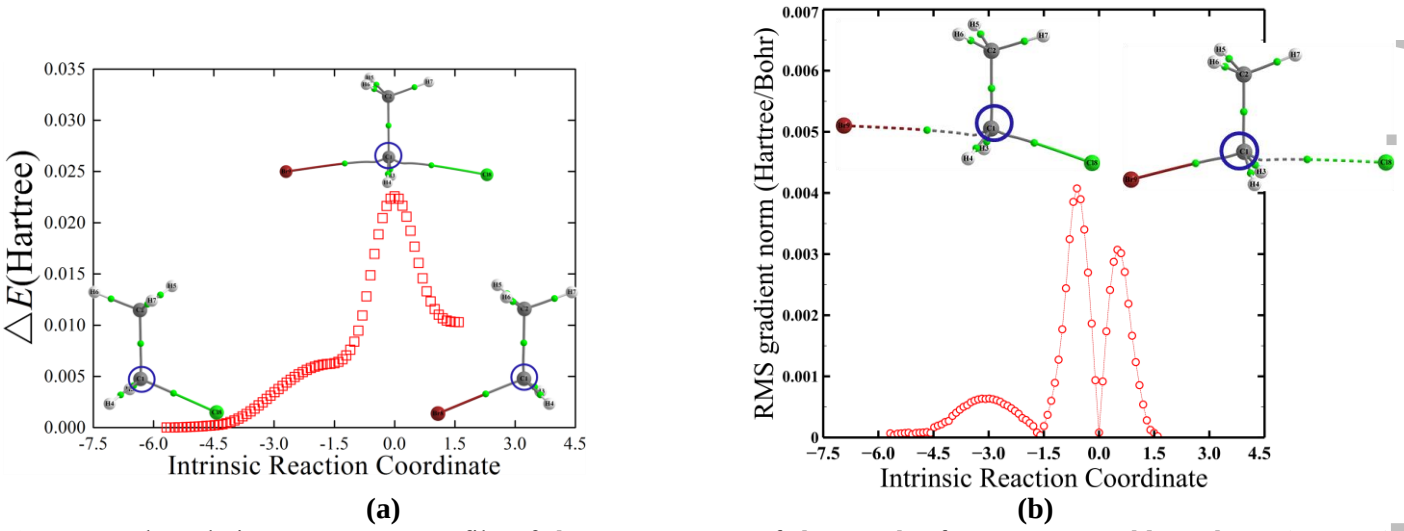

(a) **(b)**

Figure 1. The relative energy ΔE profile of the S_N2 reaction of the attack of Br^- on monochloroethane (reactant) resulting in monobromoethane (product), with Cl^- ejected as the leaving group with the transition state (TS) are presented in sub-figure **(a)**. Two intermediate structures (INTS1) and (INTS2) are located on the left and right peaks of the RMS gradient norm either side of the transition state, respectively, are presented in sub-figure **(b)**, also see **Table 1(a-b)**. The reference carbon atom C1 is highlighted by the blue circle and the green spheres indicate the bond critical points (*BCPs*).

We notice for the achiral reaction that there is a 'Walden inversion' in terms of the reversal of the $[\mathbb{C}_\sigma,\mathbb{B}_\sigma]$ assignments from the reactant monochloroethane **$[S_\sigma,R_\sigma]$** to the product monobromoethane **$[R_\sigma,S_\sigma]$**. From the reactant to the product, the helicity $\mathbb{B}_\sigma$ assignments change between **R_σ** and **S_σ** once {**R_σ**,**R_σ**,**S_σ**,**S_σ**,**S_σ**} and this occurs at the transition state, see **Table 1(b)**. For the chiral reaction there is a Walden inversion of the chirality $\mathbb{C}_\sigma$ assignments from the reactant (R)-1-chloro-1-phenylethane ($\mathbb{C}_\sigma$ = **R_σ**) to the product (S)-1-bromo-1-phenylethane ($\mathbb{C}_\sigma$ = **S_σ**) consistent with the CIP assignments, see **Table 2(b)**. For the chiral reaction the chirality $\mathbb{C}_\sigma$ assignments change once {**R_σ**,**R_σ**,**S_σ**,**S_σ**,**S_σ**} and at the transition state, see **Table 2(b)**. A slightly larger $\mathbb{C}_{helicity}$ value for the reactant (R)-1-chloro-1-phenylethane compared with the $\mathbb{C}_{helicity}$ value of the corresponding (S)-1-bromo-1-phenylethane, can be seen from their ratio (= 0.010960/0.010845 = 1.01), see **Table 2(b)**. A slightly larger $\mathbb{C}_{helicity}$ value is also found for the product (S)-1-bromo-1-phenylethane compared with the corresponding (R)-1-bromo-1-phenylethane, as seen from their ratio (=

-0.010345/-0.010274 = 1.01). Therefore, this indicates that for both the reactant and product larger $\mathbb{C}_{helicity}$ values correspond to the most preferred stereoisomer.

Table 1(a). The maximum stress tensor projections $\mathbb{T}_\sigma(s)_{max}$ = **{**bond-twist$_{max}$, bond-flexing$_{max}$, bond-anharmonicity$_{max}$} for the torsional C1-C2 *BCP* of the S_N2 reaction of the attack of Br^- on monochloroethane (reactant) resulting in monobromoethane (product), with Cl^- ejected as the leaving group including the transition state (TS) and intermediate structures (INTS1 and INTS2), see **Figure 1**: all entries have been multiplied by 10^3. The torsion θ is defined for the ranges -180.0º ≤ θ ≤ 0º clockwise (CW) and 0.0º ≤ θ ≤ 180.0º counterclockwise (CCW).

	{bond-twist$_{max}$, bond-flexing$_{max}$, bond-anharmonicity$_{max}$}	
	CW	**CCW**
SN2 reaction species		
monochloroethane	{0.648942, 1.262554, 0.902105}	{1.219886, 1.197444, 0.885461}
INTS1	{1.641014, 1.186193, 0.704935}	{1.400955, 0.968407, 0.656240}
Transition state	{1.636652, 0.805524, 0.076012}	{1.616621, 0.838184, 0.082750}
INTS2	{4.580149, 3.323640, 0.563833}	{4.783152, 3.481777, 0.617715}
monobromoethane	{1.247248, 1.350249, 0.856078}	{0.712308, 1.397459, 0.876530}

Table 1(b). The chirality $\mathbb{C}_\sigma$, helicity $\mathbb{B}_\sigma$ and the chirality-helicity measure $\mathbb{C}_{helicity}$ for the torsional C1-C2 *BCP* of the achiral S_N2 reaction of monochloroethane with Br^-, also see **Table 1(a)**. Values of the magnitude of $\mathbb{C}_\sigma$ or $\mathbb{B}_\sigma$ less than 10^{-5} indicate insignificant $\mathbb{C}_{helicity}$.

SN2 reaction species	{$\mathbb{C}_\sigma$, $\mathbb{B}_\sigma$**}**	$\mathbb{C}_{helicity}$	**[**$\mathbb{C}_\sigma$,$\mathbb{B}_\sigma$**]**
monochloroethane	{ 0.5709**[S$_\sigma$],** -0.0166**[R$_\sigma$]**}	-0.0095	**[S$_\sigma$,R$_\sigma$]**
INTS1	{-0.2401**[R$_\sigma$],** -0.0487**[R$_\sigma$]**}	0.0117	**[R$_\sigma$,R$_\sigma$]**
Transition state	{-0.0201**[R$_\sigma$],** 0.0068**[S$_\sigma$]**}	-0.0001	**[R$_\sigma$,S$_\sigma$]**
INTS2	{ 0.2030**[S$_\sigma$],** 0.0539**[S$_\sigma$]**}	0.0109	**[S$_\sigma$,S$_\sigma$]**
monobromoethane	{-0.5349**[R$_\sigma$],** 0.0205**[S$_\sigma$]**}	-0.0109	**[R$_\sigma$,S$_\sigma$]**

To compare the effects on the chirality-helicity measure $C_{helicity}$ of the substituents of the ethane molecule with the reactants and products of the formally achiral and chiral S_N2 reactions we provide the ΔE plots, ellipticity ε profiles and stress tensor trajectories $\mathbb{T}_\sigma(s)$ for ethane and 1,2-dichloroethane in the **Supplementary Materials S4**. Ethane possesses a 'staggered'-conformation for the minimum energy geometry[52] that coincides with a significant degree of chirality C_σ = 0.0514, note all values in **Tables 1-2** refer to the minimum energy geometry[52]. The 'eclipsing effect' observed in ethane is attributable to steric effects usually seen in rotational energy profiles of alkanes, in terms of maxima that are located at θ = ±60.0º and θ = ±180.0º, as also observed for conventionally chiral lactic acid and alanine[28]. There is, however, for ethane an insignificant value of the helicity $\mathbb{B}_\sigma$ (= 0.000003). The use of the helicity $\mathbb{B}_\sigma$ therefore, removes the misleading result indicated by the relatively large value of the chirality $\mathbb{C}_\sigma$ that ethane may respond to experimental techniques that utilize detectable helical motion of the bound electrons[27] similar to a conventionally chiral molecule. This is because for ethane the value of the chirality-helicity measure $\mathbb{C}_{helicity}$ ≈ 0. For 1,2-dichloroethane, the $\mathbb{C}_{helicity}$ value is also negligible, where the very low value of $\mathbb{C}_\sigma$ = -0.000114

corresponds to an absence of the eclipsing effect in the ΔE plot and $\mathbb{B}_\sigma$ = -0.000005. We note that ethane and 1,2-dichloroethane both possess significantly lower values of $\mathbb{B}_\sigma$ than the S_N2 reactants and products presented in **Table 1(b)** and **Table 2(b)**. We also provide the corresponding results for ethene and substituents where in all cases values of the chirality $\mathbb{C}_\sigma$ are low and the $\mathbb{C}_{helicity} \approx 0$ explainable by the lack of this eclipsing effect, see the **Supplementary Materials S5**.

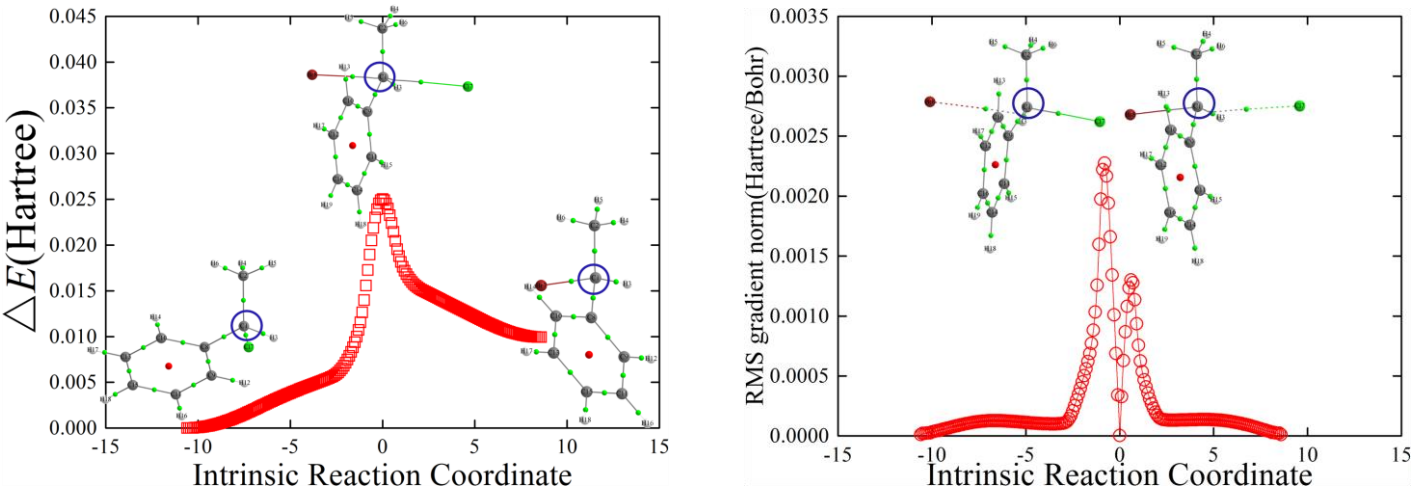

Figure 2. The relative energy ΔE profile of the S_N2 reaction of the attack of Br^- on (R)-1-chloro-1-phenylethane (reactant) resulting in (S)-1-bromo-1-phenylethane (product), with Cl^- ejected as the leaving group with the transition state are presented in sub-figure **(a)**. Two intermediate structures (INTS1) and (INTS2) are located on the left and right peaks of the RMS gradient norm either side of the transition state (TS), respectively, presented in sub-figure **(b)**, see **Table 2(a-b)**, see also the caption of **Figure 1**.

Table 2(a). The maximum stress tensor projections $\mathbb{T}_\sigma(s)_{max}$ for the torsional C1-C2 *BCP* of the chiral S_N2 reaction including the transition state (TS) and intermediate structures (INTS1 and INTS2) and stereoisomers: (S)-1-chloro-1-phenylethane and (R)-1-bromo-1-phenylethane, see **Figure 2** and the caption of **Table 1(a)**: all entries have been multiplied by 10^3.

	{bond-twist$_{max}$, bond-flexing$_{max}$, bond-anharmonicity$_{max}$}	
	CW	**CCW**
SN2 reaction species		
(R)-1-chloro-1-phenylethane	{3.831367, 6.598089, 0.977393}	{2.845538, 5.117825, 0.966354}
INTS1	{3.070597, 4.043463, 1.536603}	{2.770068, 3.271864, 1.596291}
Transition state	{3.683193, 7.762818, 0.329299}	{3.714967, 7.643615, 0.519076}
INTS2	{2.423809, 2.574118, 1.138062}	{2.619718, 3.165853, 1.116528}
(S)-1-bromo-1-phenylethane	{3.579594, 4.282447, 1.067238}	{4.308064, 5.065361, 1.053025}
Stereoisomers		
(S)-1-chloro-1-phenylethane	{2.845612, 5.117727, 0.966427}	{3.831520, 6.598219, 0.977544}
(R)-1-bromo-1-phenylethane	{4.308002, 5.065364, 1.052963}	{3.579543, 4.282547, 1.067068}

Table 2(b). The chirality $\mathbb{C}_\sigma$, helicity $\mathbb{B}_\sigma$ and the chirality-helicity measure $\mathbb{C}_{helicity}$ for the torsional C1-C2 *BCP* of the chiral S_N2 reaction, also see **Table 2(a)**.

S_N2 reaction species	$\{\mathbb{C}_\sigma, \mathbb{B}_\sigma\}$	$\mathbb{C}_{helicity}$	$[\mathbb{C}_\sigma,\mathbb{B}_\sigma]$
(R)-1-chloro-1-phenylethane	{-0.9859**[$\mathbf{R}_\sigma$]**, -0.0110**[$\mathbf{R}_\sigma$]**}	0.0108	[$\mathbf{R}_\sigma$,$\mathbf{R}_\sigma$]
INTS1	{-0.3005**[$\mathbf{R}_\sigma$]**, 0.0597**[$\mathbf{S}_\sigma$]**}	-0.0179	[$\mathbf{R}_\sigma$,$\mathbf{S}_\sigma$]
Transition state	{0.0318**[$\mathbf{S}_\sigma$]**, 0.1898**[$\mathbf{S}_\sigma$]**}	0.0060	[$\mathbf{S}_\sigma$,$\mathbf{S}_\sigma$]
INTS2	{0.1959**[$\mathbf{S}_\sigma$]**, -0.0216**[$\mathbf{R}_\sigma$]**}	-0.0042	[$\mathbf{S}_\sigma$,$\mathbf{R}_\sigma$]
(S)-1-bromo-1-phenylethane	{0.7285**[$\mathbf{S}_\sigma$]**, -0.0142**[$\mathbf{R}_\sigma$]**}	-0.0103	[$\mathbf{S}_\sigma$,$\mathbf{R}_\sigma$]
Stereoisomers			
(S)-1-chloro-1-phenylethane	{0.9859**[$\mathbf{S}_\sigma$]**, 0.0111**[$\mathbf{S}_\sigma$]**}	0.0110	[$\mathbf{S}_\sigma$,$\mathbf{S}_\sigma$]
(R)-1-bromo-1-phenylethane	{-0.7285**[$\mathbf{R}_\sigma$]**, 0.0141**[$\mathbf{S}_\sigma$]**}	-0.0103	[$\mathbf{R}_\sigma$,$\mathbf{S}_\sigma$]

Conclusions

We have detected and quantified, for the first time, the 'chirality-helicity equivalence', determined by Wang to be the origin of chirality[26], as the chirality-helicity measure $\mathbb{C}_{helicity}$, for the formally achiral and chiral S_N2 reactions of the nucleophilic attack of Br^- on chloroethane and (R)-1-chloro-1-phenylethane. We have demonstrated using the chirality-helicity measure $\mathbb{C}_{helicity}$ that both the formally achiral and chiral reactions yield a Walden-type inversion. In other words, for the chiral S_N2 reaction the products and reactants possess opposite chirality, in agreement with the optical experiment assignments i.e. S (CCW, left-handed) and R (CW, right-handed) and the CIP rules. In addition, for the chiral S_N2 reaction stereoisomers of the reactant and product possess larger $\mathbb{C}_{helicity}$ values corresponding in each case to the most energetically preferred stereoisomer. Thus, the concept of Walden inversion can be extended to achiral S_N2 reactions.

We also tracked the transition state and two intermediate structures for each reaction using the chirality-helicity measure $\mathbb{C}_{helicity}$, where CIP assignments cannot be used due to the five-fold coordination of the chiral carbon atom. In doing so we discovered unexpected chirality in the absence of stereoisomers: for the transition state and two intermediate structures of the chiral reaction and the entire achiral reaction profile. We have also demonstrated using the $\mathbb{C}_{helicity}$ measure of ethane why the chirality $\mathbb{C}_\sigma$ measure alone is insufficient for formally achiral species particularly where steric effects due to eclipsed conformations are important. We check this finding with substituted ethane in addition to ethene and substituted ethene and find consistency.

S_N2 reactions represent one of the most basic building blocks for understanding more complex asymmetric reactions. Thus, this is a very important first step in quantifying such unified chirality measures, with these results providing a foundation for more complex reaction pathways. On the basis of the $\mathbb{C}_{helicity}$ values we expect that photoexcitation circular dichroism experiments will detect the effects of chirality for the species of the formally achiral S_N2 reaction. The chirality-helicity $\mathbb{C}_{helicity}$ measure provides a global

chirality measure of the degree of the helical displacement of the torsional *BCP*, consistent with photoexcitation circular dichroism experiments on neutral molecules that utilize the helical motion of the bound electrons. This work therefore indicates the need for more photoexcitation circular dichroism experiments to detect undiscovered chirality in formally achiral molecules and reaction species. We have provided a new picture of chirality in terms of the electron density by constructing the $\mathbb{C}_{helicity}$ from stress tensor trajectories $\mathbb{T}_{\sigma}(s)$ in a manner that is predictive, fully quantifiable and consistent with recent experiments[27,29].

Future work could include application to chiral selectivity during a chemical reaction, in particular for the design of reactions with post-transition state bifurcations (PTSB) where an asynchronous nitrene insertion into C–C σ bonds can be used to modulate the product sensitivity[53].

Further work could include the determination of the $\mathbb{C}_{helicity}$ for molecules with multiple chiral centers: each dominant torsional bond associated with a separate chiral center would be considered independently. Treating the chiral centers independently is possible because obtaining the $\mathbb{C}_{helicity}$ requires constraining the corresponding torsional dihedral angle, allowing the remaining atoms and molecular electronic density distribution to relax to an energetic minimum in response. Future applications could include chiral catalysis and the prediction of asymmetric synthetic reactions of all intermediates where CIP assignments cannot be used. Therefore, it is very attractive to apply the idea of this investigation to the prediction of asymmetric synthetic reactions, which is one of the most fundamental problems in industrial organic and catalytic chemistry[33,34].

Supporting Information

1. Supplementary Materials S1. NG-QTAIM and stress tensor theoretical background and procedure to generate the stress tensor trajectories $\mathbb{T}_{\sigma}(s)$.

2. Supplementary Materials S2. $\mathbb{T}_{\sigma}(s)$ of the torsional C1-C2 *BCP* in the achiral S_N2 reaction.

3. Supplementary Materials S3. $\mathbb{T}_{\sigma}(s)$ of the torsional C1-C2 *BCP* in the chiral S_N2 reaction.

4. Supplementary Materials S4. $\mathbb{T}_{\sigma}(s)$ of the torsional C1-C2 *BCP* of ethane and substituted ethane.

5. Supplementary Materials S5. $\mathbb{T}_{\sigma}(s)$ of the torsional C1-C2 *BCP* of ethene and substituted ethene.

Acknowledgements

The National Natural Science Foundation of China is gratefully acknowledged, project approval number: 21673071. The One Hundred Talents Foundation of Hunan Province is also gratefully acknowledged for the support of S.J. and S.R.K. H.F. and T.v.M. gratefully acknowledge computational support via the EaStCHEM Research Computing Facility. This research was also enabled in part by computational support

provided by Compute Ontario (www.computeontario.ca), SHARCNET (www.sharcnet.ca) and Compute Canada (www.computecanada.ca) by the kind auspices of our sponsor Paul W. Ayers. We thank H. Rzepa for useful discussions, recommendations on calculation parameters and archived data. Martin Quack is thanked for providing relevant publications.

References

[1] R. S. Cahn, C. Ingold, V. Prelog, *Angew. Chem. Int. Ed. Engl.* **1966**, *5*, 385–415.
[2] V. Prelog, G. Helmchen, *Angew. Chem. Int. Ed. Engl.* **1982**, *21*, 567–583.
[3] R. M. Hanson, S. Musacchio, J. W. Mayfield, M. J. Vainio, A. Yerin, D. Redkin, *J. Chem. Inf. Model.* **2018**, *58*, 1755–1765.
[4] V. Prelog, *Croat. Chem. Acta* **2006**, *79*, 49-57 (XLIX-LVII).
[5] L. Pasteur, *Ann Chim Phys* **1850**, *28*, 56–99.
[6] N. Katsonis, F. Lancia, D. A. Leigh, L. Pirvu, A. Ryabchun, F. Schaufelberger, *Nat. Chem.* **2020**, *12*, 939–944.
[7] S. M. Morrow, A. J. Bissette, S. P. Fletcher, *Nat. Nanotechnol.* **2017**, *12*, 410–419.
[8] J. E. Hein, D. G. Blackmond, *Acc. Chem. Res.* **2012**, *45*, 2045–2054.
[9] J. L. Bada, *Nature* **1995**, *374*, 594–595.
[10] R. Breslow, Z.-L. Cheng, *Proc. Natl. Acad. Sci.* **2009**, *106*, 9144–9146.
[11] G. Pályi, C. Zucchi, L. Caglioti, Eds. , *Progress in Biochirality*, Elsevier Science, ISBN 978-0-08-044396-6, **2004**.
[12] Y. Chen, K. Deng, S. Lei, R. Yang, T. Li, Y. Gu, Y. Yang, X. Qiu, C. Wang, *Nat. Commun.* **2018**, *9*, 2711.
[13] W. A. Bonner, *Orig. Life Evol. Biosph.* **1991**, *21*, 59–111.
[14] R. Wallace, *C. R. Biol.* **2011**, *334*, 263–268.
[15] N. A. Hawbaker, D. G. Blackmond, *Nat. Chem.* **2019**, *11*, 957–962.
[16] X. Chen, M. Boero, O. Lopez-Acevedo, *Phys. Rev. Mater.* **2020**, *4*, 065601.
[17] Y. Hu, S. J. Teat, W. Gong, Z. Zhou, Y. Jin, H. Chen, J. Wu, Y. Cui, T. Jiang, X. Cheng, W. Zhang, *Nat. Chem.* **2021**, *13*, 660–665.
[18] H. Flack, *Acta Crystallogr. Sect. A* **2009**, *65*, 371–389.
[19] M. Quack, in *Proc. 240 Conf. -Sci. Gt. Chall.* (Eds.: A.R. Dinner, S.A. Rice), John Wiley & Sons, Ltd, **2014**, pp. 247–291.
[20] R. Berger, M. Quack, *ChemPhysChem* **2000**, *1*, 57–60.
[21] A. Fresnel, *Mém. Académie Sci. Inst. Fr.* **1821**, *7*, 45–176.
[22] J. H. Brewster, in *Stereochem. I*, Springer, Berlin, Heidelberg, **1974**, pp. 29–71.
[23] L. Rosenfeld, *Z. Für Phys.* **1929**, *52*, 161–174.
[24] D. J. Caldwell, H. Eyring, T. Y. Chang, *Phys. Today* **1972**, *25*, 53.
[25] I. Tinoco, R. W. Woody, *J. Chem. Phys.* **1964**, *40*, 160–165.
[26] D. Zhigang Wang, *Mendeleev Commun.* **2004**, *14*, 244–247.
[27] S. Beaulieu, A. Comby, D. Descamps, B. Fabre, G. A. Garcia, R. Géneaux, A. G. Harvey, F. Légaré, Z. Mašín, L. Nahon, A. F. Ordonez, S. Petit, B. Pons, Y. Mairesse, O. Smirnova, V. Blanchet, *Nat. Phys.* **2018**, *14*, 484–489.
[28] T. Xu, J. H. Li, R. Momen, W. J. Huang, S. R. Kirk, Y. Shigeta, S. Jenkins, *J. Am. Chem. Soc.* **2019**, *141*, 5497–5503.
[29] K. Banerjee-Ghosh, O. Ben Dor, F. Tassinari, E. Capua, S. Yochelis, A. Capua, S.-H. Yang, S. S. P. Parkin, S. Sarkar, L. Kronik, L. T. Baczewski, R. Naaman, Y. Paltiel, *Science* **2018**, *360*, 1331–1334.
[30] K. C. Harper, M. S. Sigman, *Science* **2011**, *333*, 1875–1878.
[31] M. H. Garner, C. Corminboeuf, *Chem. Commun.* **2021**, *57*, 6408–6411.
[32] R. F. W. Bader, *Atoms in Molecules: A Quantum Theory*, Oxford University Press, USA, New York, **1994**.
[33] D. K. Kondepudi, K. Asakura, *Acc. Chem. Res.* **2001**, *34*, 946–954.
[34] A. Matsumoto, H. Ozaki, S. Tsuchiya, T. Asahi, M. Lahav, T. Kawasaki, K. Soai, *Org. Biomol. Chem.* **2019**, *17*, 4200–4203.

[35] R. F. W. Bader, *J. Chem. Phys.* **1980**, *73*, 2871–2883.
[36] T. Xu, S. R. Kirk, S. Jenkins, *Chem. Phys. Lett.* **2020**, *738*, 136907.
[37] M. X. Hu, T. Xu, R. Momen, A. Azizi, S. R. Kirk, S. Jenkins, *Chem. Phys. Lett.* **2017**, *677*, 156–161.
[38] W. J. Huang, T. Xu, S. R. Kirk, M. Filatov, S. Jenkins, *Chem. Phys. Lett.* **2018**, *713*, 125–131.
[39] J. H. Li, W. J. Huang, T. Xu, S. R. Kirk, S. Jenkins, *Int. J. Quantum Chem.* **2018**, *119*, e25847.
[40] H. Guo, A. Morales-Bayuelo, T. Xu, R. Momen, L. Wang, P. Yang, S. R. Kirk, S. Jenkins, *J. Comput. Chem.* **2016**, *37*, 2722–2733.
[41] P. Yang, T. Xu, R. Momen, A. Azizi, S. R. Kirk, S. Jenkins, *Int. J. Quantum Chem.* **2018**, *118*, e25565.
[42] T. Xu, L. Wang, Y. Ping, T. van Mourik, H. Früchtl, S. R. Kirk, S. Jenkins, *Int. J. Quantum Chem.* **2018**, *118*, e25676.
[43] T. Xu, J. Farrell, R. Momen, A. Azizi, S. R. Kirk, S. Jenkins, D. J. Wales, *Chem. Phys. Lett.* **2017**, *667*, 25–31.
[44] T. A. Keith, *AIMAll, Revision 19.10.12*, TK Gristmill Software, Overland Park KS, USA, **2019**.
[45] H. Nakatsuji, *J. Am. Chem. Soc.* **1974**, *96*, 24–30.
[46] R. G. A. Bone, R. F. W. Bader, *J. Phys. Chem.* **1996**, *100*, 10892–10911.
[47] S. Jenkins, M. I. Heggie, *J. Phys. Condens. Matter* **2000**, *12*, 10325–10333.
[48] P. W. Ayers, S. Jenkins, *J. Chem. Phys.* **2009**, *130*, 154104-154104–11.
[49] T. Tian, T. Xu, S. R. Kirk, I. T. Rongde, Y. B. Tan, S. Manzhos, Y. Shigeta, S. Jenkins, *Phys. Chem. Chem. Phys.* **2020**, *22*, 2509–2520.
[50] Michael J. Frisch, G. W. Trucks, H. Bernhard Schlegel, Gustavo E. Scuseria, Michael A. Robb, James R. Cheeseman, Giovanni Scalmani, Vincenzo Barone, Benedetta Mennucci, G. A. Petersson, H. Nakatsuji, M. Caricato, Xiaosong Li, H. P. Hratchian, Artur F. Izmaylov, Julien Bloino, G. Zheng, J. L. Sonnenberg, M. Hada, M. Ehara, K. Toyota, R. Fukuda, J. Hasegawa, M. Ishida, T. Nakajima, Y. Honda, O. Kitao, H. Nakai, T. Vreven, J. A. Montgomery Jr., J. E. Peralta, François Ogliaro, Michael J. Bearpark, Jochen Heyd, E. N. Brothers, K. N. Kudin, V. N. Staroverov, Rika Kobayashi, J. Normand, Krishnan Raghavachari, Alistair P. Rendell, J. C. Burant, S. S. Iyengar, Jacopo Tomasi, M. Cossi, N. Rega, N. J. Millam, M. Klene, J. E. Knox, J. B. Cross, V. Bakken, C. Adamo, J. Jaramillo, R. Gomperts, R. E. Stratmann, O. Yazyev, A. J. Austin, R. Cammi, C. Pomelli, J. W. Ochterski, R. L. Martin, K. Morokuma, V. G. Zakrzewski, G. A. Voth, P. Salvador, J. J. Dannenberg, S. Dapprich, A. D. Daniels, Ö. Farkas, J. B. Foresman, J. V. Ortiz, J. Cioslowski, D. J. Fox, *Gaussian 09, Revision E.01*, Gaussian, Inc., 340 Quinnipiac St Bldg 40 Wallingford, CT 06492 USA, **2009**.
[51] H. S. Rzepa, "IRC pathways for SN2 reactions, Imperial College Research Data Repository, 2021," can be found under DOI: 10.14469/hpc/7900, **2021**.
[52] Wu Judy I-Chia, Schleyer Paul von Ragué, *Pure Appl. Chem.* **2013**, *85*, 921.
[53] R. B. Campos, D. J. Tantillo, *Chem* **2019**, *5*, 227–236.

10.1002/cphc.202100397

For Table of Contents only